

## **Fluid Flow through Parallel Plates in the Presence of Hall Current with Inclined Magnetic Field in a Rotating System**

\*Rina Perven, \*\*Md. Mahmud Alam

Mathematics Discipline, Science, Engineering and Technology School  
Khulna University, Khulna-9208, Bangladesh  
(rina\_math1@yahoo.com; alam\_mahmud2000@yahoo.com)

### **Abstract**

This investigation related with the study of the influence of hall current of a viscous incompressible electrically conducting free convection fluid flow, through the parallel plates in a rotating system under the action of inclined magnetic field. It is considered that the channel is being rotated with uniform angular velocity about an axis normal to the plates. To obtain the dimensionless momentum, and induction equations, usual non-dimensional variables have been used. The explicit finite difference technique has been used for numerical solution. The stability conditions and convergence criteria of the explicit finite difference scheme are established for finding the restriction of the values of various parameters to get more accuracy. The effects of these parameters have been explained by the figures of local and average shear stress and current density at the moving plate.

### **Key words**

Inclined magnetic field, Hall current, Rotating system, Current density, Finite Difference Techniques

### **Nomenclature**

$q$ :	Fluid velocity	$\theta$ :	Angle of inclination
$P'$ :	Fluid pressure including centrifugal force	$\sigma$ :	Electrical conductivity of the fluid

$\mathbf{J}$ :	Current density	$\rho$ :	Fluid density
$\mathbf{\Omega}$ :	Angular velocity	$\mu$ :	Co-efficient of viscosity
$t$ :	Time	$\mu_e$ :	Magnetic permeability
$\tau$ :	Dimensionless time	$\omega_e$ :	Cyclotron frequency
$\hat{k}$ :	Unit vector along $z$ -axis	$\tau_e$ :	Electron collision time
$u$ :	Velocity component in the $x$ -direction	$\nu$ :	Co-efficient of kinematic viscosity
$v$ :	Velocity component in the $y$ -direction	$\rho$ :	Density of the fluid in the boundary layer
$w$ :	Velocity component in the $z$ -direction	$B_x$ :	Primary inclined Magnetic field
$\eta$ :	Stressing factor	$B_y$ :	Secondary inclined Magnetic field
$L$ :	Length of the boundary layer	$R$ :	Rotation parameter
$\nabla$ :	Differential operator	$m$ :	Hall parameter
$\mathbf{E}$ :	Electric field	$M^2$ :	Magnetic parameter
$\mathbf{B}$ :	Magnetic induction vector	$P_g$ :	Constant pressure gradient
$B_0$ :	Magnetic flux	$P_m$ :	Magnetic parameter

## 1. Introduction

The study of MHD free convection fluid flow through parallel plates in the presence of inclined magnetic field with hall current in a rotating system has become in several industrial processes, scientific and engineering fields. Magnetic inclination is the angle that the geomagnetic field is tilted with respect to the surface of the earth. Magnetic inclination varies from  $90^0$ (perpendicular to the surface) at the magnetic poles to  $0^0$  (parallel to the surface) at the magnetic equator. An inclined magnetic field is just a magnetic field with a nonzero inclination. In astrophysics, they usually mean the radial direction. The radial direction means the normal (perpendicular) direction to the surface (of the Sun etc.). Non-inclined magnetic field is radial; an inclined magnetic field has field lines that are twisted around the Sun (or another object) a little bit. To summarize, the adjective "inclined" doesn't carry any special physical content - it just refers to the geometrical arrangement of the objects relatively to the field. **Haque et al. (2009)**, observed Transient heat and mass transfer by mixed convection flow from a vertical porous plate with induced magnetic field, constant heat and mass fluxes. The Hall Effect is the production of a

voltage difference across an electrical conductor, transverse to an electric current in the conductor and a magnetic field perpendicular to the current. It is well known that, the effect of Hall current become significant at low density of an ionized fluid as stated by **Cowling (1957)**. In the case of an electrically conducting rotating gas at low pressure, there has an interaction of the magnetic field with the electric field of both the electrons and the ionized atoms of the gas. If the magnetic field is perpendicular to the electric field, a current is induced in the conductive rotating gas whose direction is perpendicular to the both the electric field and the magnetic field. **Sutton and Sherman (1965)** investigated the hydrodynamic flow of a viscous ionized gas between two parallel plates taking Hall effects into account. The Hall effects on an unsteady MHD free convection heat and mass transfer flow through a porous medium near an infinite vertical porous plate with constant heat flux have been analyzed by **Sattar and Alam (1995)**. **Crammer K.R. and Pai S.I., (1973)** studied the influence of electromagnetic force. Hall effects on MHD flow in a rotating channel in the presence of inclined magnetic field have been investigated by **Ghosh and Bhattacharjee (2000)**. **Edmad *et al.* (2005)** studied the effects of Hall current on magneto hydrodynamic free convection flow past a semi-infinite vertical plate with mass transfer. Micropolar fluid behaviours on unsteady MHD heat and Mass transfer flow with constant heat and mass fluxes, joule heating and viscous dissipation has been investigated by **Ziaul Haque *et al.* (2011)**. The combined effect of Hall and ion-slip currents on unsteady MHD Couette flows in a rotating system has been investigated by **Jha and Apere (2010)**. **Seth *et al.* (2010)** studied the Hartmann flow in a rotating system in the presence of inclined magnetic field with Hall effects. Our aim is to investigate numerically the fluid flow through a rotating system in the presence of inclined magnetic field with hall current. In this study the two-dimensional case with hall current has been considered. The governing equations of the problem contain a system of partial differential equations which are transformed by usual transformation into a non-dimensional system of non-linear coupled partial differential equations. The obtained systems are solved numerically by a finite difference method. The effects of some well known parameters have been verified by analyzing the figures of local and average shear stresses and current densities at the moving plate.

## 2. Mathematical model of the flow

A flow model of the fluid flow is considered for a rotating system in the presence of inclined magnetic field with hall current. It is also assumed that, the flow is between two parallel horizontal plates in where the lower plate is fixed. Introducing the Cartesian coordinate system, the  $x$  –axis is chosen along the plates in horizontal direction of the flow and  $z$  –axis is normal to it. Both the fluid and the channel are in a state of rigid body rotation with uniform angular velocity  $\Omega$  about  $z$  –axis. The fluid is permeated by a uniform magnetic flux density  $B_0$  applied in a direction, which is inclined at an angle  $\theta$  with the positive direction of  $z$  –axis in  $xz$  –plane. The physical configuration and coordinate system of the present investigation are shown in the following Figs. 1 and 2.

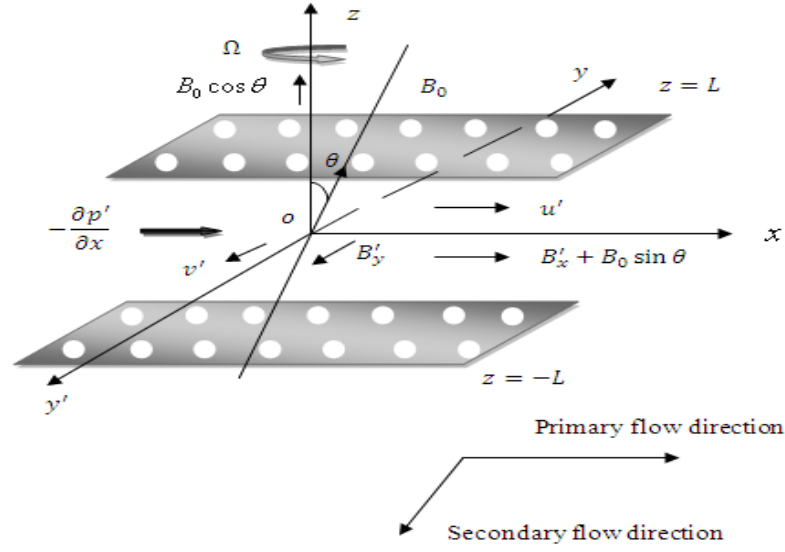


Fig.1. Physical representation of the problem

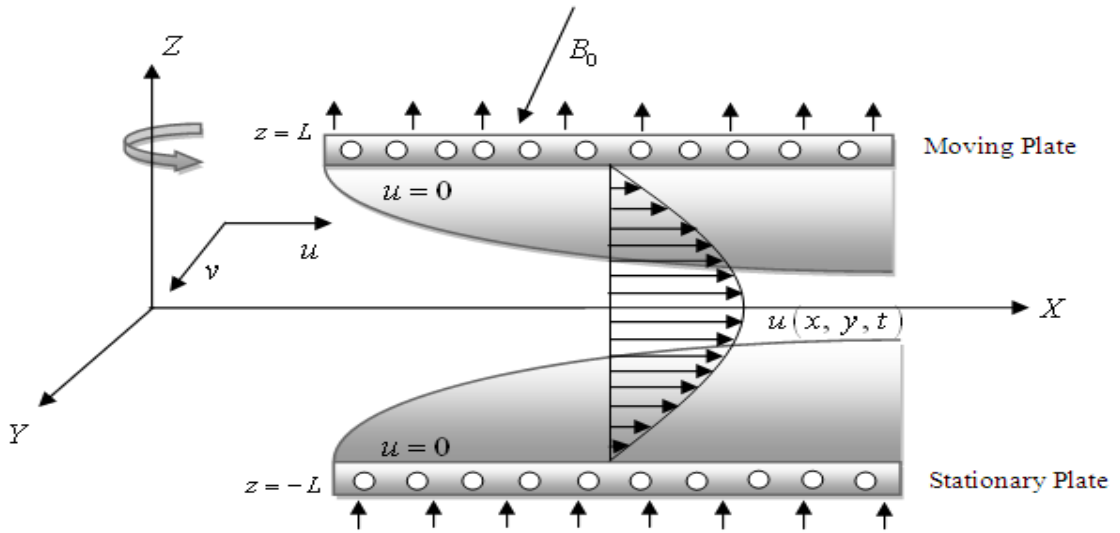


Fig.2. Geometrical configuration and coordinate system

Within the framework of the above stated assumptions relevant to the two-dimensional problem are governed by the following system of coupled non-linear partial differential equations.

**Continuity equation**

$$\frac{\partial u'}{\partial x} + \frac{\partial w'}{\partial z} = 0 \quad (1)$$

**Momentum equation**

$$\frac{\partial u'}{\partial t} + u' \frac{\partial u'}{\partial x} + w' \frac{\partial u'}{\partial z} - 2\Omega v' = -\frac{1}{\rho} \frac{dp'}{dx} + \nu \frac{\partial^2 u'}{\partial z^2} + \frac{1}{\mu_e \rho} B_0 \cos \theta \frac{\partial B'_x}{\partial z} \quad (2)$$

$$\frac{\partial v'}{\partial t} + u' \frac{\partial v'}{\partial x} + w' \frac{\partial v'}{\partial z} + 2\Omega u' = \nu \frac{\partial^2 v'}{\partial z^2} + \frac{1}{\mu_e \rho} B_0 \cos \theta \frac{\partial B'_y}{\partial z} \quad (3)$$

### Magnetic Induction equation

$$\frac{\partial B'_x}{\partial t} = B_0 \cos \theta \frac{\partial u'}{\partial z} + \frac{1}{\sigma \mu_e} \frac{\partial^2 B'_x}{\partial z^2} + \frac{m}{\sigma \mu_e} \cos \theta \frac{\partial^2 B'_y}{\partial z^2} \quad (4)$$

$$\frac{\partial B'_y}{\partial t} = B_0 \cos \theta \frac{\partial v'}{\partial z} + \frac{1}{\sigma \mu_e} \frac{\partial^2 B'_y}{\partial z^2} - \frac{m}{B_0 \sigma \mu_e} \left[ B_0 \cos \theta \frac{\partial^2 B'_x}{\partial z^2} + \frac{\partial B'_x}{\partial x} \frac{\partial B'_x}{\partial z} \right] \quad (5)$$

The corresponding boundary conditions for the problem are;

$$u' = 0, \quad v' = 0, \quad \frac{\partial B'_x}{\partial z} = 0, \quad \frac{\partial B'_y}{\partial z} = 0 \quad \text{at } z = \pm L \quad \text{for } t \geq 0 \quad (6)$$

### 3. Solution

Since the solutions of the governing equations under the initial and boundary conditions will be based on a finite difference method, it is required to make the said equations dimensionless.

For this purpose the following dimensionless variables are introduced as;

$$\xi = \frac{x}{L}, \quad \eta = \frac{z}{L}, \quad u = \frac{u'L}{\nu}, \quad v = \frac{v'L}{\nu}, \quad w = \frac{w'L}{\nu}, \quad p = \frac{L^2 p'}{\rho \nu^2}, \quad B_x = \frac{B'_x}{\sigma \mu_e \nu B_0}, \quad B_y = \frac{B'_y}{\sigma \mu_e \nu B_0}, \quad \tau = \frac{t U_0^2}{\nu}$$

After simplification the equations (1)-(5) with corresponding boundary condition (6), the following nonlinear coupled partial differential equations are obtained in terms of dimensionless variables;

$$\frac{\partial u}{\partial \xi} + \frac{\partial w}{\partial \eta} = 0 \quad (7)$$

$$\frac{\partial u}{\partial \tau} + u \frac{\partial u}{\partial \xi} + w \frac{\partial u}{\partial \eta} - 2Rv = \frac{\partial^2 u}{\partial \eta^2} + P_{r_g} + M^2 \cos \theta \frac{\partial B_x}{\partial \eta} \quad (8)$$

$$\frac{\partial v}{\partial \tau} + u \frac{\partial v}{\partial \xi} + w \frac{\partial v}{\partial \eta} + 2Ru = \frac{\partial^2 v}{\partial \eta^2} + M^2 \cos \theta \frac{\partial B_y}{\partial \eta} \quad (9)$$

$$P_m \frac{\partial B_x}{\partial \tau} = \cos \theta \frac{\partial u}{\partial \eta} + \frac{\partial^2 B_x}{\partial \eta^2} + m \cos \theta \frac{\partial^2 B_y}{\partial \eta^2} \quad (10)$$

$$P_m \frac{\partial B_y}{\partial \tau} = \cos \theta \frac{\partial v}{\partial \eta} + \frac{\partial^2 B_y}{\partial \eta^2} - m \left[ \cos \theta \frac{\partial^2 B_x}{\partial \eta^2} + P_m \frac{\partial B_x}{\partial \xi} \frac{\partial B_x}{\partial \eta} \right] \quad (11)$$

The dimensionless boundary conditions are;

$$u = 0, \quad v = 0, \quad \frac{\partial B_x}{\partial \eta} = 0, \quad \frac{\partial B_y}{\partial \eta} = 0 \quad \text{at } \eta = \pm 1 \quad \text{for } t \geq 0; \quad (12)$$

where  $\tau$  represents the dimensionless time,  $\xi$  and  $\eta$  are the dimensionless Cartesian coordinates,  $u, v$  and  $w$  are the dimensionless velocity components,  $B_x, B_y$  are the dimensionless primary and secondary inclined magnetic fields. Here,

$R = \frac{\Omega L^2}{\nu}$  is **rotation parameter** which is reciprocal of Ekman number,

$P_{r_g} = -\frac{\partial p}{\partial \xi}$  is non-dimensional **constant pressure gradient**,

$M^2 = \frac{B_0^2 L^2 \sigma}{\rho \nu}$  is **magnetic parameter** which is square of Hartmann number.

$P_m = \sigma \mu_e \nu$  is **magnetic Prandtl number**.

$m = \omega_e \tau_e$  is the **hall parameter**.

### 3.1 Shear stress and Current density

The quantities of chief physical interest on various parameters are local and average shear stress. The following equations represent the local and average shear stress at the plate.

For primary velocity, the local shear stress,  $\tau_L = \mu \left( \frac{\partial u'}{\partial z} \right)_{z=0}$  and the average shear stress,

$$\tau_A = \mu \int \left( \frac{\partial u'}{\partial z} \right)_{x=0} dx \text{ which are proportional to } \left( \frac{\partial u}{\partial \eta} \right)_{\eta=0} \text{ and } \int_0^{100} \left( \frac{\partial u}{\partial \eta} \right)_{\eta=0} d\xi \text{ respectively.}$$

For secondary velocity, the local shear stress,  $\tau_L = \mu \left( \frac{\partial v'}{\partial z} \right)_{z=0}$  and the average shear stress,

$$\tau_A = \mu \int \left( \frac{\partial v'}{\partial z} \right)_{z=0} dx \text{ which are proportional to } \left( \frac{\partial v}{\partial \eta} \right)_{\eta=0} \text{ and } \int_0^{100} \left( \frac{\partial v}{\partial \eta} \right)_{\eta=0} d\xi \text{ respectively.}$$

From the inclined magnetic field, the effects of various parameters on local and average current density have been calculated. The following equations represent the local and average current density at the plate.

The local current density  $J_L = \mu \left( -\frac{\partial B'_x}{\partial z} \right)_{z=0}$  in  $x$ -direction and the average current density

$$J_A = \mu \int \left( -\frac{\partial B'_x}{\partial z} \right)_{z=0} dx \text{ in } x\text{-direction are proportional to } \left( -\frac{\partial B_x}{\partial \eta} \right)_{\eta=0} \text{ and } \int_0^{100} \left( -\frac{\partial B_x}{\partial \eta} \right)_{\eta=0} d\xi$$

respectively. The local current density  $J_L = \mu \left( -\frac{\partial B'_y}{\partial z} \right)_{z=0}$  and

the average current density  $J_A = \mu \int \left( -\frac{\partial B'_y}{\partial z} \right)_{z=0} dx$  in  $y$ -direction are proportional to

$$\left( -\frac{\partial B_y}{\partial \eta} \right)_{\eta=0} \text{ and } \int_0^{100} \left( -\frac{\partial B_y}{\partial \eta} \right)_{\eta=0} d\xi \text{ respectively.}$$

### 3.2 Numerical Technique

For simplicity the explicit finite difference method has been used to solve equations (7) - (11) subject to the conditions given by (12). To obtain the solution of the difference equations, the region of the flow is divided into a grid of lines parallel to  $\xi$  and  $\eta$  axes where  $\xi$ -axes is taken along the plates and  $\eta$  axes is normal to the plates. Here the plate is considered of height  $\xi_{\max} = 100$  i.e.  $\xi$  varies from 0 to 100 and regard  $\eta_{\max} = 2$  i.e.  $\eta$  varies from

-1 to 1. There are  $m=44$  and  $n=44$  grid spacing in the  $\xi$  and  $\eta$  directions respectively and taken as follows,  $\Delta\xi = 2.273(0 \leq \xi \leq 44)$ ,  $\Delta\eta = 0.0455(-1 \leq \eta \leq 1)$  with the smaller time step,  $\Delta\tau = 0.001$ . These mesh steps are shown in Fig.3.

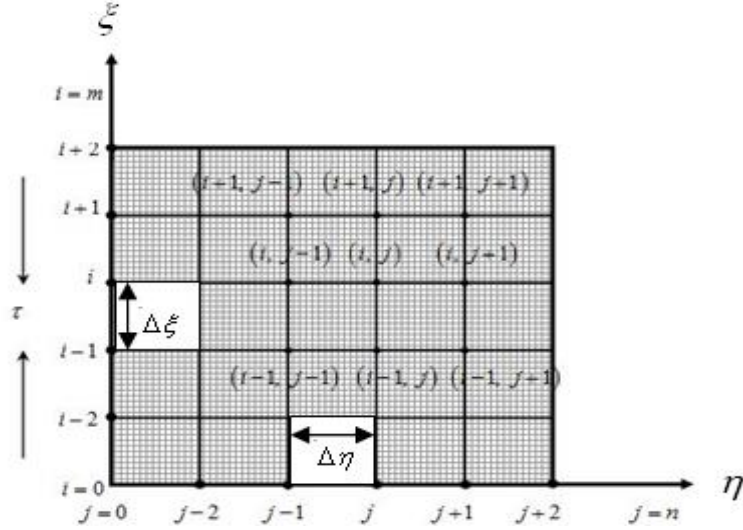


Fig.3. Explicit finite difference system grid

Let  $u', v', B'_x$  and  $B'_y$  denote the values of  $u, v, B_x$  and  $B_y$  at the end of a time-step respectively. Using explicit **finite difference approximation** for the partial differential equation, Eqs. (7) - (11) are obtained in the form of an appropriate set of finite difference equations.

$$\frac{u_{i,j} - u_{i-1,j}}{\Delta\xi} + \frac{w_{i,j+1} - w_{i,j}}{\Delta\eta} = 0 \quad (13)$$

$$\frac{u'_{i,j} - u_{i,j}}{\Delta\tau} + u_{i,j} \frac{u_{i,j} - u_{i-1,j}}{\Delta\xi} + w_{i,j} \frac{u_{i,j+1} - u_{i,j}}{\Delta\eta} - 2Rv_{i,j} = \frac{u_{i,j+1} - 2u_{i,j} + u_{i,j-1}}{(\Delta\eta)^2} + P_{r_g} + M^2 \cos\theta \frac{B_{x_{i,j+1}} - B_{x_{i,j}}}{\Delta\eta} \quad (14)$$

$$\frac{v'_{i,j} - v_{i,j}}{\Delta\tau} + u_{i,j} \frac{v_{i,j} - v_{i-1,j}}{\Delta\xi} + w_{i,j} \frac{v_{i,j+1} - v_{i,j}}{\Delta\eta} + 2Ru_{i,j} = \frac{v_{i,j+1} - 2v_{i,j} + v_{i,j-1}}{(\Delta\eta)^2} + M^2 \sin\theta \frac{B_{y_{i,j+1}} - B_{y_{i,j}}}{\Delta\eta} \quad (15)$$

$$P_m \frac{B'_{x_{i,j}} - B_{x_{i,j}}}{\Delta\tau} = \cos\theta \frac{u_{i,j+1} - u_{i,j}}{\Delta\eta} + \frac{B_{x_{i,j+1}} - 2B_{x_{i,j}} + B_{x_{i,j-1}}}{(\Delta\eta)^2} + m \cos\theta \frac{B_{y_{i,j+1}} - 2B_{y_{i,j}} + B_{y_{i,j-1}}}{(\Delta\eta)^2} \quad (16)$$

$$P_m \frac{B'_{y_{i,j}} - B_{y_{i,j}}}{\Delta\tau} = \cos\theta \frac{v_{i,j+1} - v_{i,j}}{\Delta\eta} + \frac{B_{y_{i,j+1}} - 2B_{y_{i,j}} + B_{y_{i,j-1}}}{(\Delta\eta)^2} - m \cos\theta \frac{B_{x_{i,j+1}} - 2B_{x_{i,j}} + B_{x_{i,j-1}}}{(\Delta\eta)^2} - mP_m \frac{B_{x_{i,j+1}} - B_{x_{i,j}}}{\Delta\eta} \frac{B_{x_{i,j}} - B_{x_{i-1,j}}}{\Delta\xi} \quad (17)$$

with the boundary conditions;

$$u_{i,j} = 0, v_{i,j} = 0, B'_{x_{i,j}} = 0, B'_{y_{i,j}} = 0 \text{ at } \eta = \pm 1 \text{ for } t \geq 0 \quad (18)$$

Here the subscripts  $i$  and  $j$  designate the grid points with  $\xi$  and  $\eta$  coordinates respectively. During any one time step, the coefficients  $u_{i,j}, v_{i,j}, B_{x_{i,j}}, B_{y_{i,j}}$  appearing in equations (13), (14), (15), (16) and (17) are created as constants. Then at the end of any time-step  $\Delta\tau$  the new primary velocity  $u'$ , secondary velocity  $v'$  and the new induced magnetic fields  $B'_x, B'_y$  at all interior nodal points may be obtained by successive applications of the above finite difference equations. This process is repeated in time and provided the time-step is sufficiently small,  $u', v', B'_x, B'_y$  should eventually converge to values which approximate the steady-state solution of equations (13), (14), (15), (16) and (17).

The effects of relevant parameters have been verified by analyzing the figures of local and average shear stresses and current density at the plates of channel. The numerical values of the local shear stresses and local current density are evaluated by **Five-point** approximate formula and the average shear stresses and average current density are calculated by the **Simpson's  $\frac{1}{3}$**  integration rule. The obtained values are graphically shown in Figs. 4-51.

#### 4. Stability and convergence analysis

The stability conditions of the finite difference method are;

$$\left| \frac{2\Delta\tau}{(\Delta\eta)^2} \times \frac{1}{P_m} \right| \leq 1$$

And convergence limitation of the problem is  $P_m \geq 0.966$ .

#### 5. Results and Discussion

Using the numerical values of the equations of this model obtained by finite difference technique, the graphs of non-dimensional primary velocity ( $u$ ), secondary velocity ( $v$ ), primary inclined magnetic field ( $B_x$ ), secondary inclined magnetic field ( $B_y$ ) distribution within the boundary layer have been computed for different values of various parameters. To observe the physical situation of the problem, the steady-state solutions have been illustrated in Figs. 4-51. To obtain the steady-state solutions, the computation has been carried out up to  $\tau = 80$ . The behavior of different parameters on primary velocity, secondary velocity and inclined magnetic fields are justified by the effect of local and average shear stresses and current densities on these parameters i.e. rotation parameter ( $R$ ), hall parameter ( $m$ ), magnetic parameter ( $M^2$ ),

magnetic prandtl number ( $P_m$ ), constant pressure gradient ( $P_{r_g}$ ) and angle of inclination ( $\theta$ ) in case of moving plate.

For this purpose the numerical solutions of the above mentioned quantities for those parameters are computed and the obtained values are plotted in Figs. 4-51.

Figures 4-27 are represented for local case of shear stresses and current densities in case of moving plate.

The steady-state local shear -stress and local current density profiles for different values of  $R$  in case of moving plate are shown in Figs.4-7. As displayed in Figs. 4 and 5, the local shear stress in  $x$  and  $y$  – direction show a decreasing effect with the increase of  $R$ . But the local current density profiles in  $x$  and  $y$ –directions have an increasing effect with the rise of  $R$ , as shown in Figs. 6-7.

Figures 8-11 are shown for the effect of hall parameter  $m$  on local shear stresses and local current densities in case of moving plate. As represented in Figs. 8 and 9, the local shear stress in  $x$  and  $y$  – direction there has a decreasing effect on  $m$ . From Figs. 10 and 11, it can be observed that the local current density in  $x$  – direction has increasing effect while the local current density profiles in  $y$  – direction decrease with the increase of hall parameter.

The displayed Figs. 12-15 show the effect of magnetic parameter  $M^2$  on local shear stresses and current densities in case of moving plate. Figures 12 and 13 represent that local shear stresses in  $x$  and  $y$  – direction show increasing effect. The local current density profiles in  $x$  and  $y$  – directions show decreasing effect with the increase of  $M^2$  as in Figs. 14 and 15.

The curve of local shear stresses and local current densities in case of moving plate are presented in Figs. 16-19 for magnetic prandtl number  $P_m$ . The local shear stress in  $x$  – direction shows a increasing effect as seen in Fig. 16, while the local shear stress profiles in  $y$  – direction decrease slightly with  $P_m$  as plotted in Fig.17. The local current density profiles in  $x$  – direction show minor effect with the increase of  $P_m$  according to Fig. 18. In Fig. 19, the local current density profiles in  $y$  – direction show increasing effect on  $P_m$ .

Figures 20-23 are shown for the effect of constant pressure gradient ( $P_{r_g}$ ) in case of moving plate.

The local shear stress in  $x$  – direction shows an increasing effect on the rise of  $P_{r_g}$  as in Fig. 20. But the local shear stress in  $y$  – direction and local current density in  $x$  – direction have a decreasing effect as displayed in Figs. 21 and 22. Again the local current density in  $y$  – direction has an increasing effect as displayed in Figs. 23.

The profiles of steady state local shear stresses and local current densities in case of moving plate for different values of angle of inclination ( $\theta$ ) are represented in Fig. 24-27. The local shear stresses in  $x$  and  $y$  – direction shows a decreasing effect as seen in Figs. 24 and 25. But in Figs.

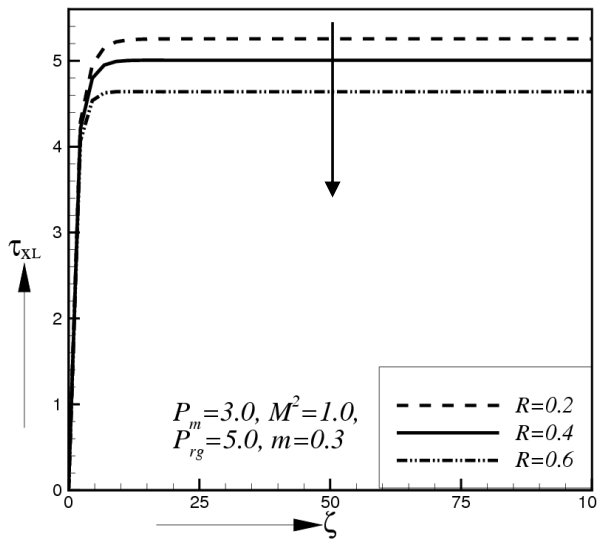


Fig.4. Steady-state local shear stress in  $x$  – direction for different values of  $R$  at  $\theta = 45^\circ$  in case of moving plate

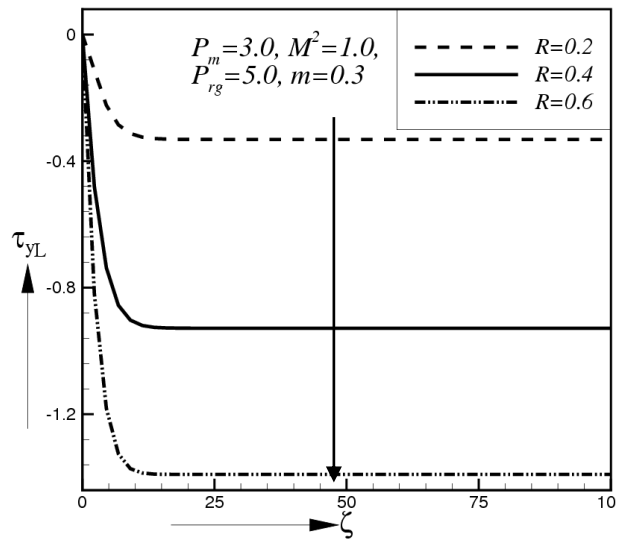


Fig.5. Steady-state local shear stress in  $y$  – direction for different values of  $R$  at  $\theta = 45^\circ$  in case of moving plate

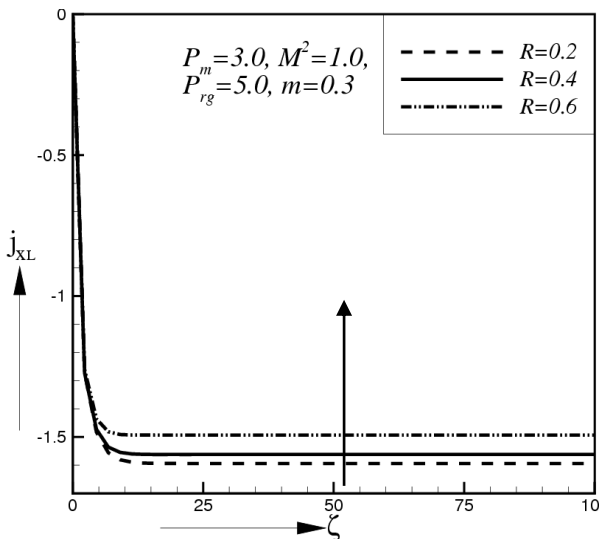


Fig.6. Steady-state local current density in  $x$  – direction for different values of  $R$  at  $\theta = 45^\circ$  in case of moving plate

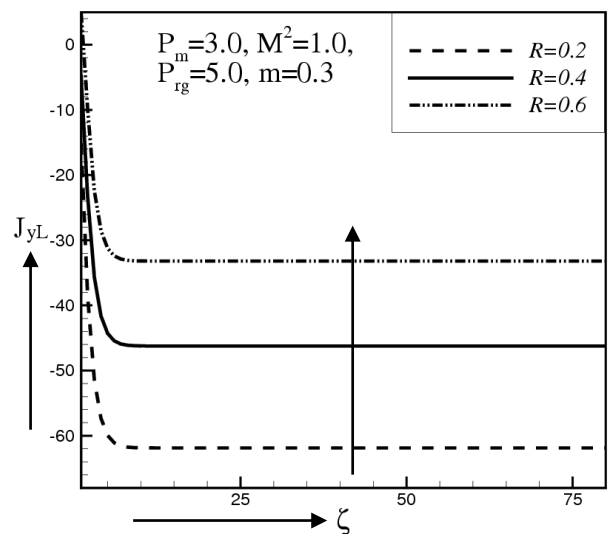


Fig.7. Steady-state local current density in  $y$  – direction for different values of  $R$  at  $\theta = 45^\circ$  in case of moving plate

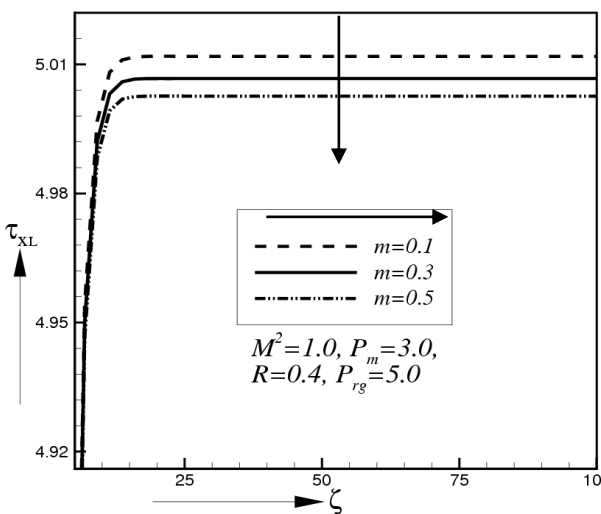


Fig.8. Steady-state local shear stress in  $x$  – direction for different values of  $m$  at  $\theta = 45^\circ$  in case of moving plate

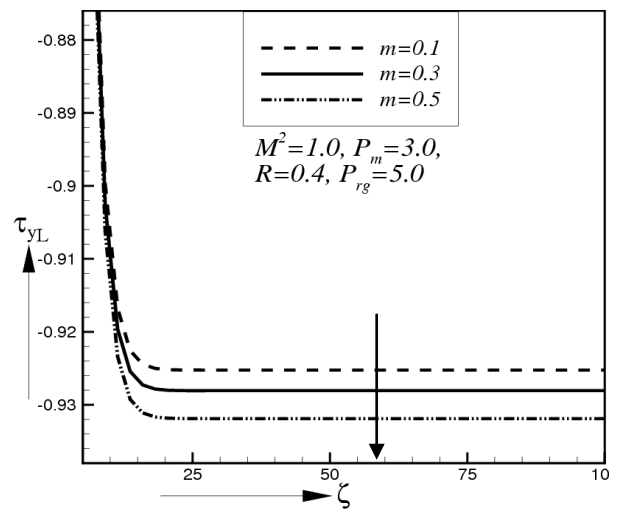


Fig.9. Steady-state local shear stress in  $y$  – direction for different values of  $m$  at  $\theta = 45^\circ$  in case of moving plate

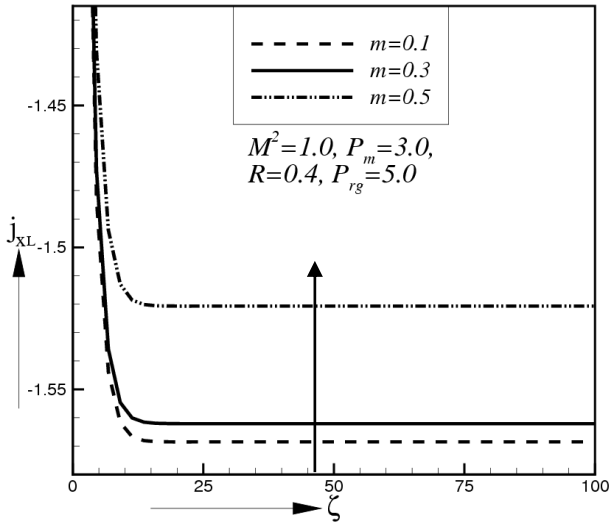


Fig.10. Steady-state local current density in  $x$  – direction for different values of  $m$  at  $\theta = 45^\circ$  in case of moving plate

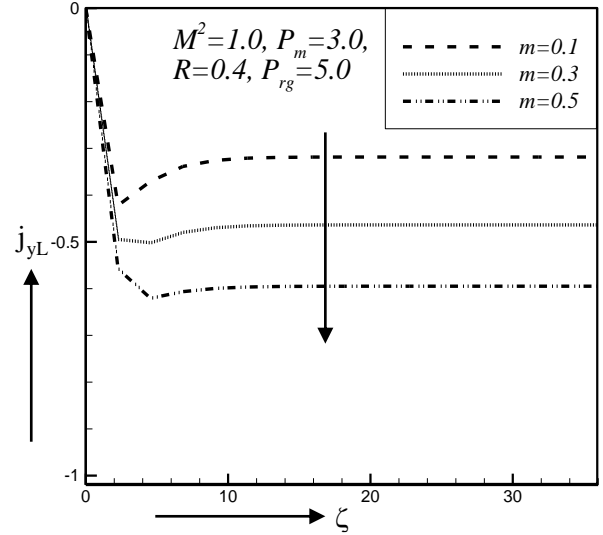


Fig.11. Steady-state local current density in  $y$  – direction for different values of  $m$  at  $\theta = 45^\circ$  in case of moving plate

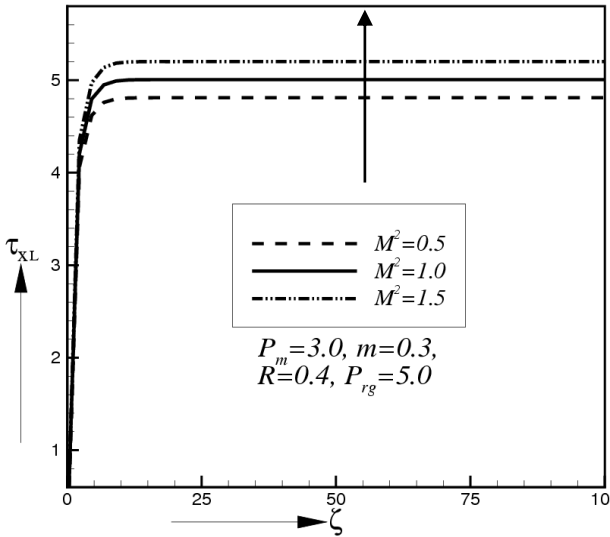


Fig.12. Steady-state local shear stress in  $x$  – direction for different values of  $M^2$  at  $\theta = 45^\circ$  in case of moving plate

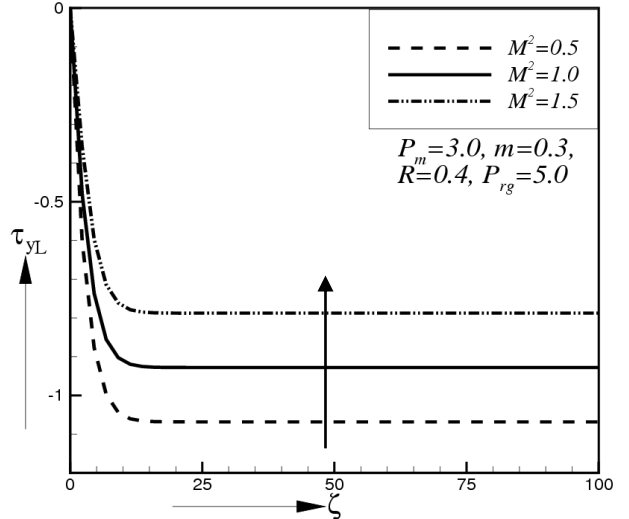


Fig.13. Steady-state local shear stress in  $y$  – direction for different values of  $M^2$  at  $\theta = 45^\circ$  in case of moving plate

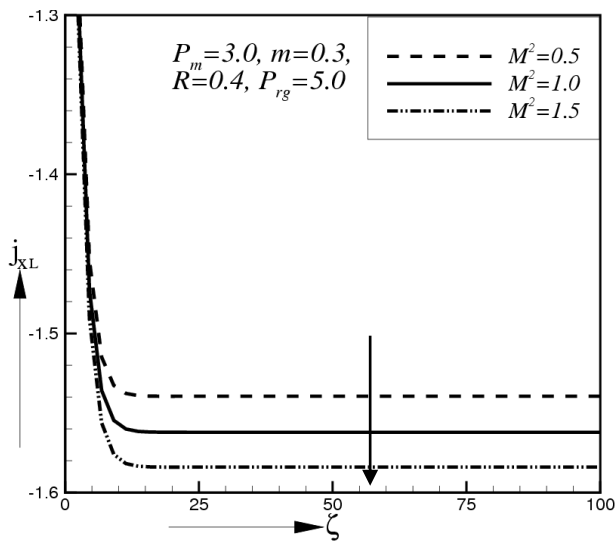


Fig.14. Steady-state local current density in  $x$  – direction for different values of  $M^2$  at  $\theta = 45^\circ$  in case of moving plate

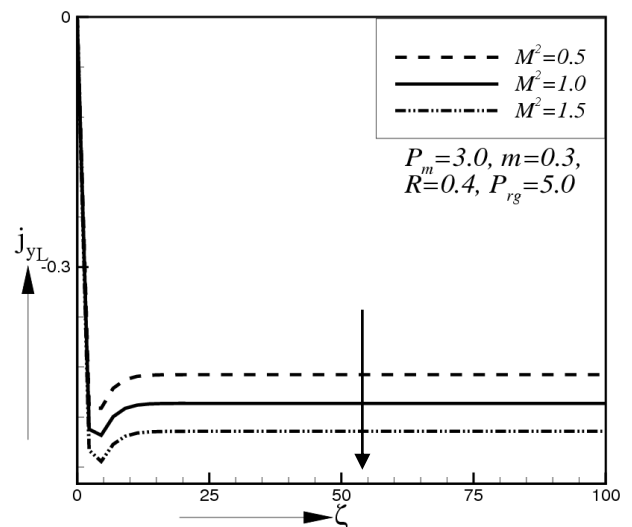


Fig.15. Steady-state local current density in  $y$  – direction for different values of  $M^2$  at  $\theta = 45^\circ$  in case of moving plate

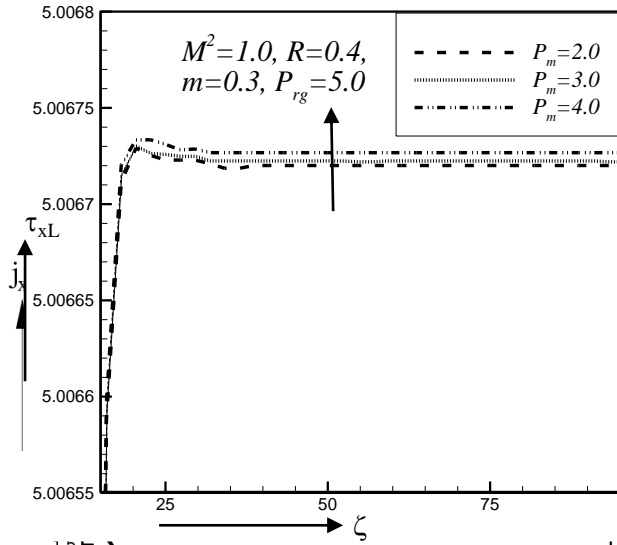


Fig.16. Steady-state local shear stress in  $x$  – direction for different values of  $P_m$  at  $\theta = 45^\circ$  in case of moving plate

Fig.18. Steady-state local current density in  $x$  – direction for different values of  $P_m$  at  $\theta = 45^\circ$  in case of moving plate

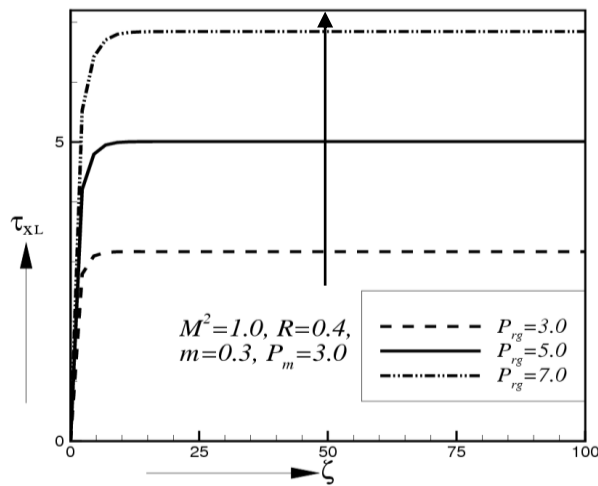


Fig.20. Steady-state local shear stress in  $x$  – direction for different values of  $P_{rg}$  at  $\theta = 45^\circ$  in case of moving plate

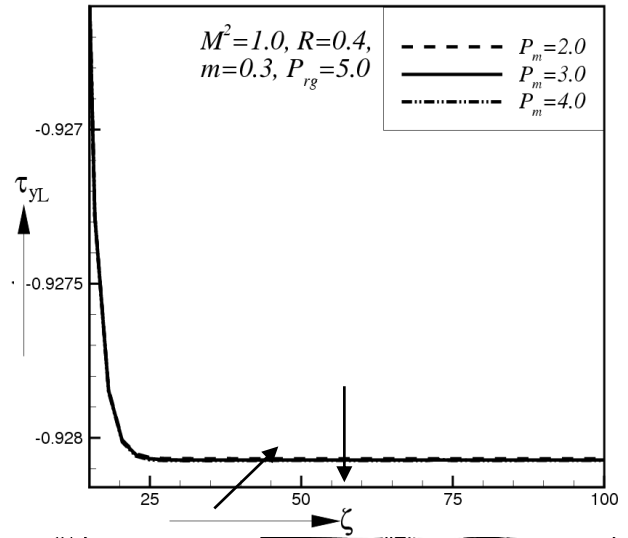
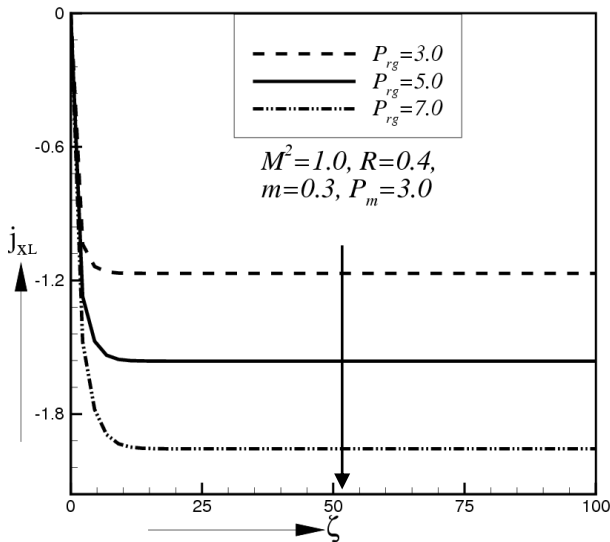


Fig.17. Steady-state local shear stress in  $y$  – direction for different values of  $P_m$  at  $\theta = 45^\circ$  in case of moving plate

Fig.19. Steady-state local current density in  $y$  – direction for different values of  $P_m$  at  $\theta = 45^\circ$  in case of moving plate

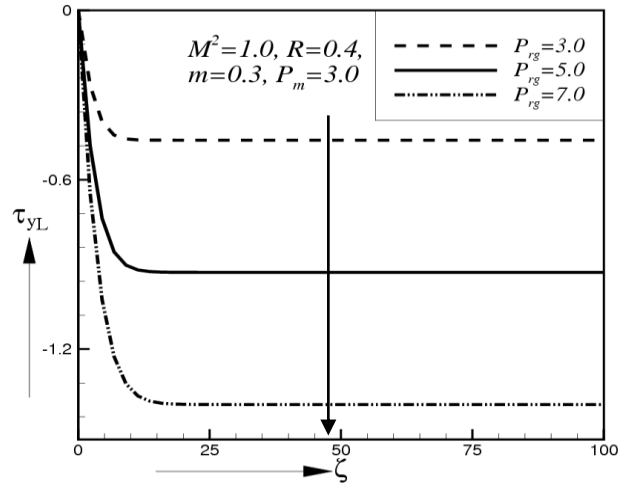


Fig.21. Steady-state local shear stress in  $y$  – direction for different values of  $P_{rg}$  at  $\theta = 45^\circ$  in case of moving plate

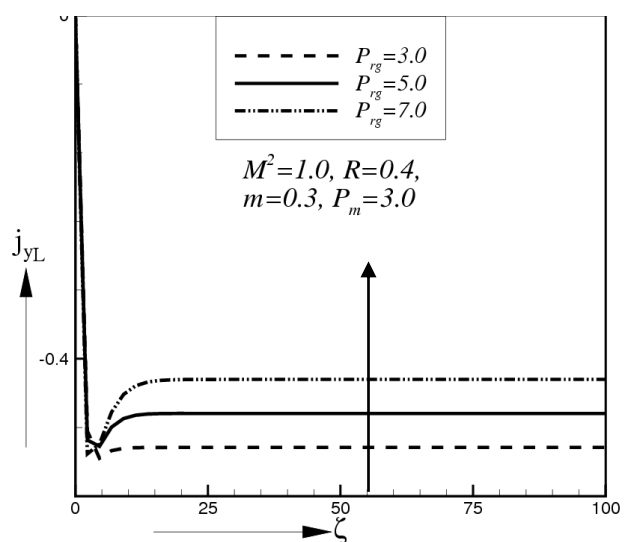


Fig.22. Steady-state local current density in  $x$  – direction for different values of  $P_{rg}$  at  $\theta = 45^\circ$  in case of moving plate

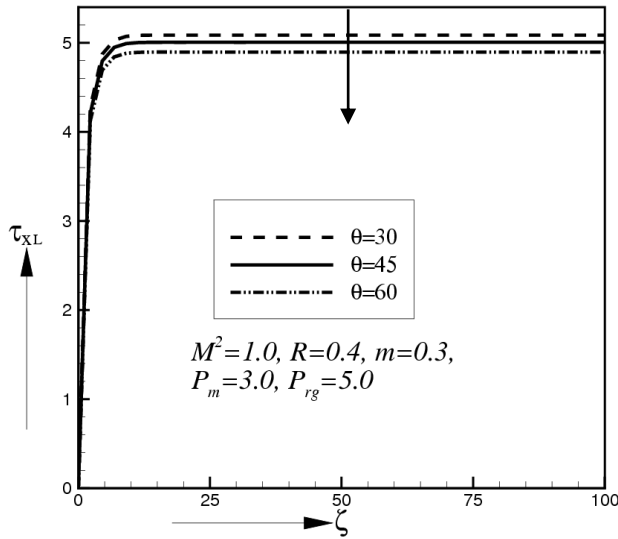


Fig.24. Steady-state local shear stress in  $x$  – direction for different values of  $\theta$  in case of moving plate

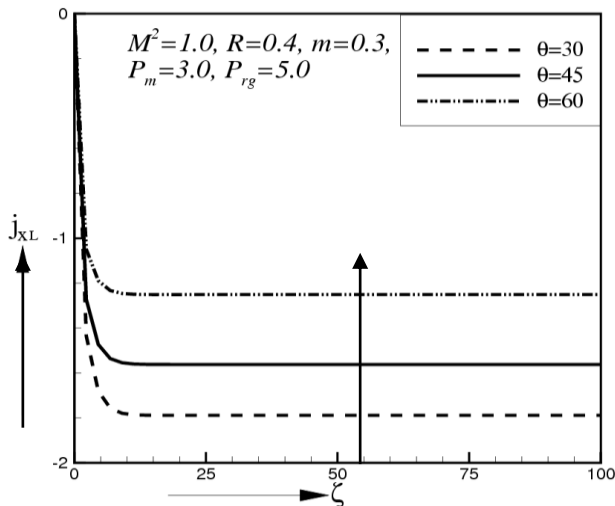


Fig.26. Steady-state local current density in  $x$  – direction for different values of  $\theta$  in case of moving plate

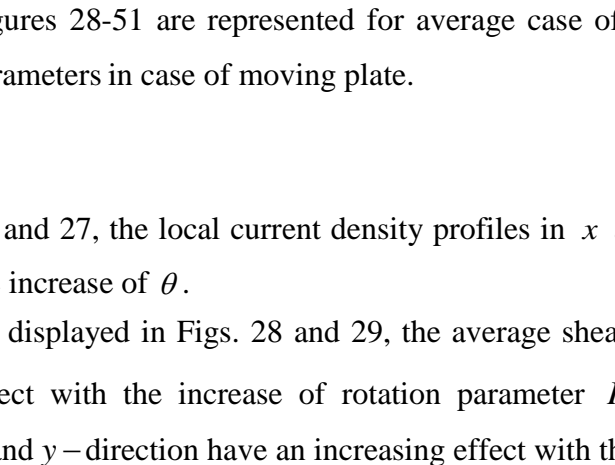


Fig.23. Steady-state local current density in  $y$  – direction for different values of  $P_{rg}$  at  $\theta = 45^\circ$  in case of moving plate

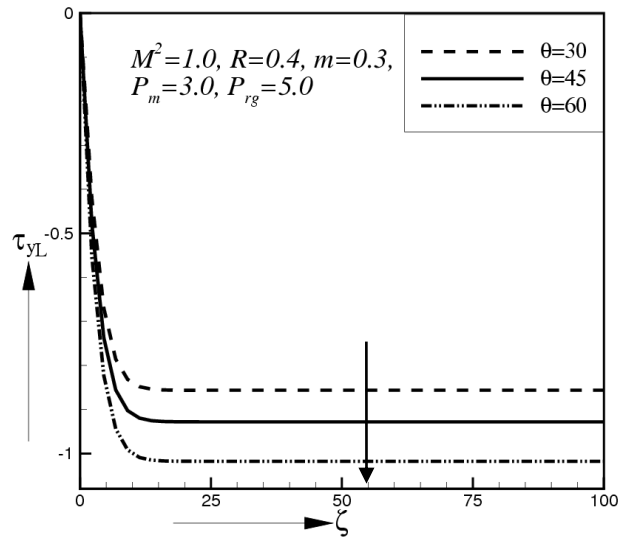


Fig.25. Steady-state local shear stress in  $y$  – direction for different values of  $\theta$  in case of moving plate

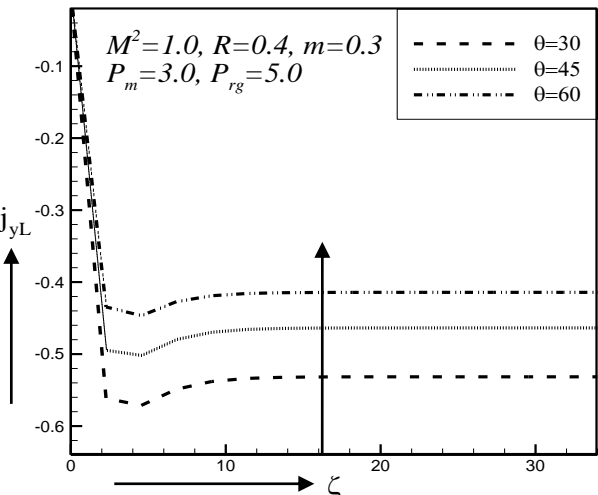


Fig.27. Steady-state local current density in  $y$  – direction for different values of  $\theta$  in case of moving plate

Figures 28-51 are represented for average case of shear stresses and current densities on various parameters in case of moving plate.

26 and 27, the local current density profiles in  $x$  and  $y$  – direction show an increasing effect with the increase of  $\theta$ .

As displayed in Figs. 28 and 29, the average shear stress in  $x$  and  $y$  – direction show a decreasing effect with the increase of rotation parameter  $R$ . But the average current density profiles in  $x$  and  $y$  – direction have an increasing effect with the rise of  $R$  as shown in Figs. 30 and 31.

Figures 32-35 are shown for the effect of hall parameter  $m$  on average shear stresses and average current densities in case of moving plate. As represented in Figs. 32 and 33, the average shear stress in  $x$  and  $y$ -direction has a decreasing effect on  $m$ . From Figs. 34 and 35, it can be observed that the average current density profiles in  $x$ -direction has increasing effect while the average current density profiles in  $y$ -direction decrease with the increase of hall parameter.

Figures 36 and 37 represent that the average shear stress in  $x$  and  $y$ -direction show increasing effect for magnetic parameter  $M^2$ . The average current density profiles in  $x$  and  $y$ -direction show decreasing effect with the increase of  $M^2$  as in Figs. 38 and 39.

The average shear stress in  $x$  and  $y$ -direction show a decreasing effect before  $\tau < 10$  (approx.) and after this they have minor effect on the magnetic prandtl number  $P_m$  as seen in Figs. 40 and 41. From Fig. 42, the average current density profiles in  $x$ -direction show cross-flow effect i.e. increase before  $\tau < 20$  (approx.) and then the reverse effect occurs. The average current density profiles in  $y$ -direction have an increasing effect on  $P_m$  as in Fig. 43.

The average shear stress in  $x$ -direction shows an increasing effect on the rise of constant pressure gradient  $(P_{r_g})$  as in Fig. 44. As displayed in Figs. 45, and 46, the average shear stress in  $y$ -direction and current density in  $x$ -direction have a decreasing effect but there has an increasing effect for current density in  $y$ -direction on  $(P_{r_g})$  as in Fig. 47.

The profiles of steady state average shear stresses and current densities in case of moving plate for different values of angle of inclination  $\theta$  are represented in Figs. 48-51. The average shear stresses in  $x$  and  $y$ -direction show a decreasing effect with  $\theta$  as seen in Figs. 48 and 49. As in Figs. 50 and 51, the average current density profiles in both  $x$  and  $y$ -direction show an increasing effect with the increase of  $\theta$ .

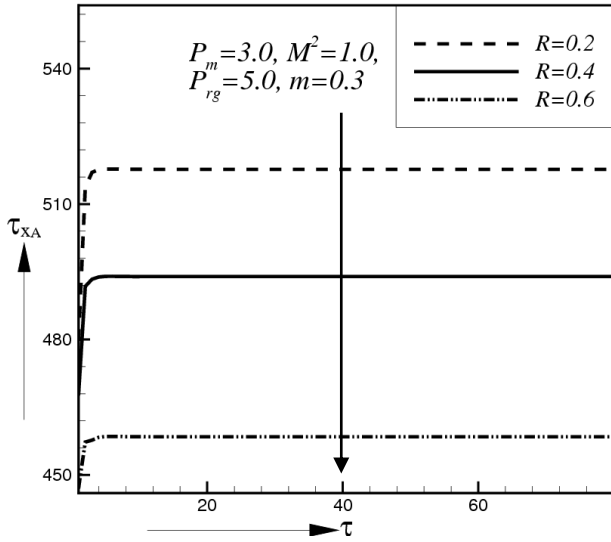


Fig.28. Steady-state average shear stress in  $x$  – direction for different values of  $R$  at  $\theta = 45^\circ$  in case of moving plate

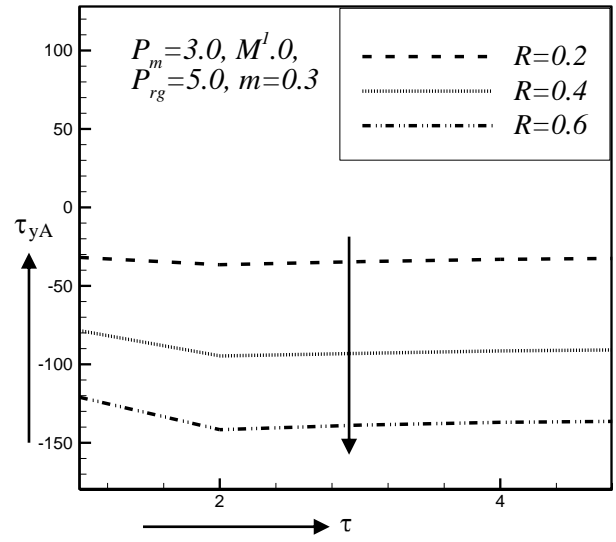


Fig.29. Steady-state average shear stress in  $y$  – direction for different values of  $R$  at  $\theta = 45^\circ$  in case of moving plate

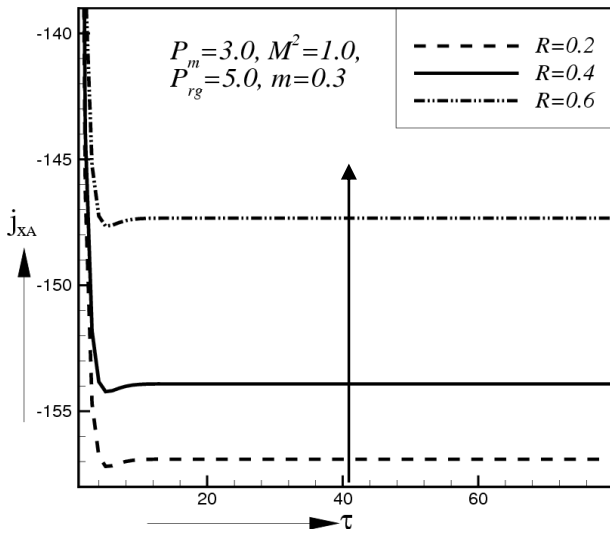


Fig.30. Steady-state average current density in  $x$  – direction for different values of  $R$  at  $\theta = 45^\circ$  in case of moving plate

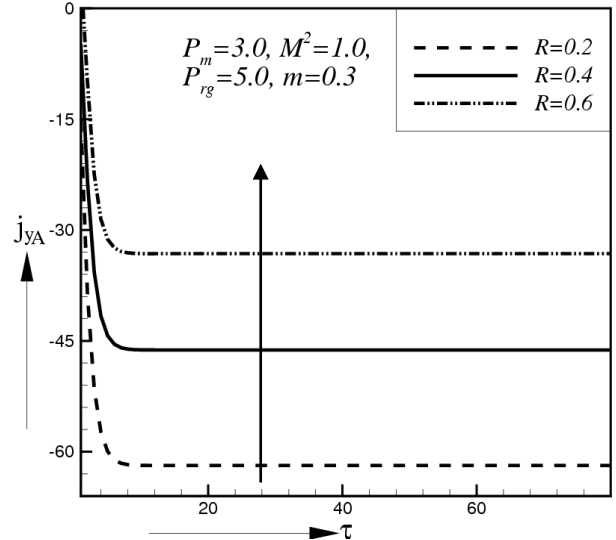


Fig.31. Steady-state average current density in  $y$  – direction for different values of  $R$  at  $\theta = 45^\circ$  in case of moving plate

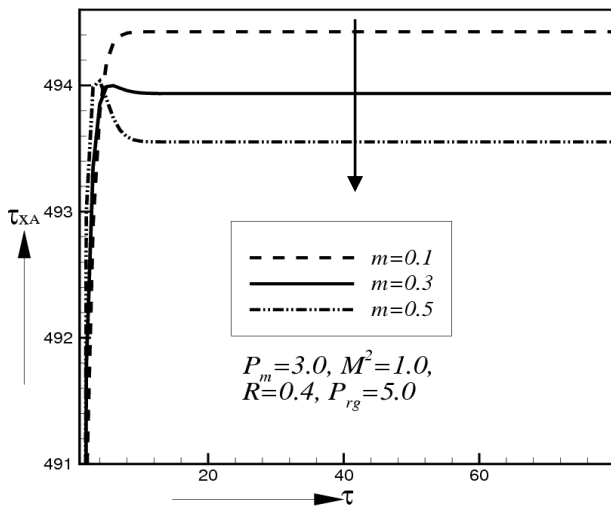


Fig.32. Steady-state average shear stress in  $x$  – direction for different values of  $m$  at  $\theta = 45^\circ$  in case of moving plate

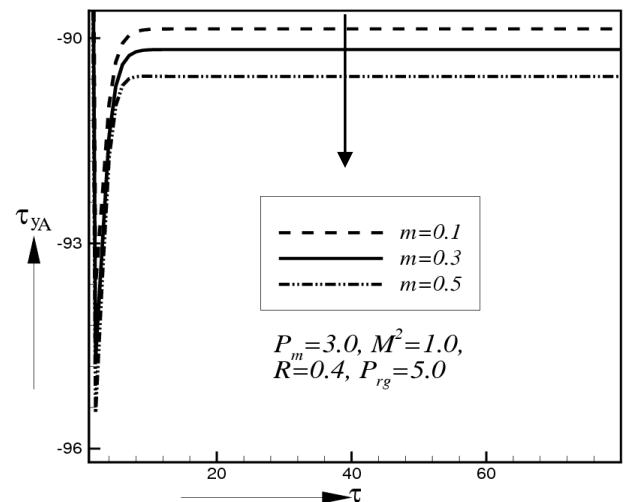


Fig.33. Steady-state average shear stress in  $y$  – direction for different values of  $m$  at  $\theta = 45^\circ$  in case of moving plate

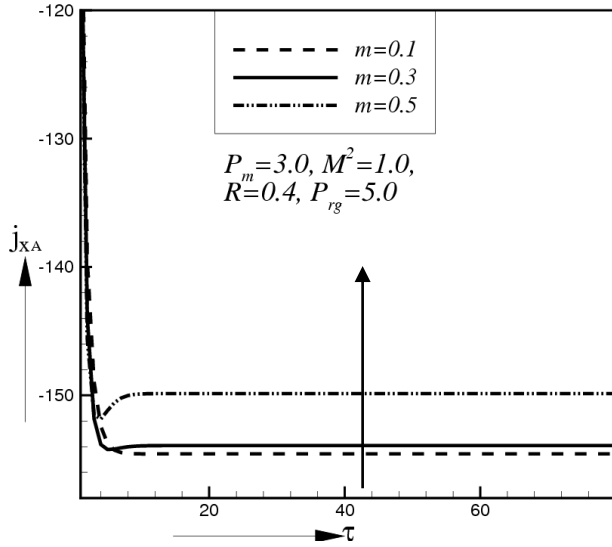


Fig.34. Steady-state average current density in  $x$  – direction for different values of  $m$  at  $\theta = 45^\circ$  in case of moving plate

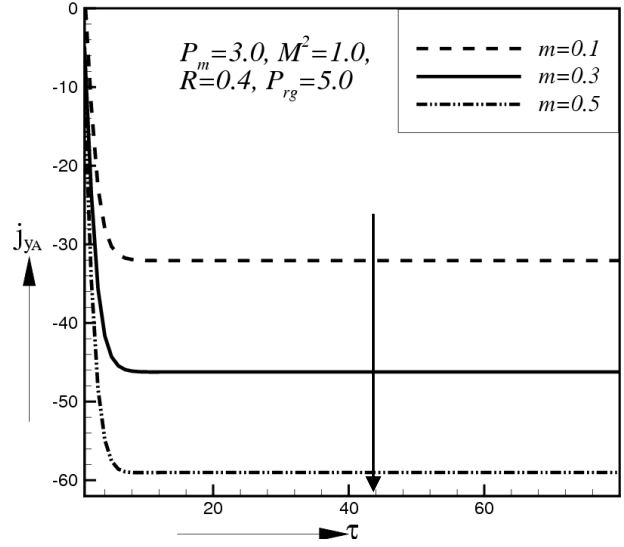


Fig.35. Steady-state average current density in  $y$  – direction for different values of  $m$  at  $\theta = 45^\circ$  in case of moving plate

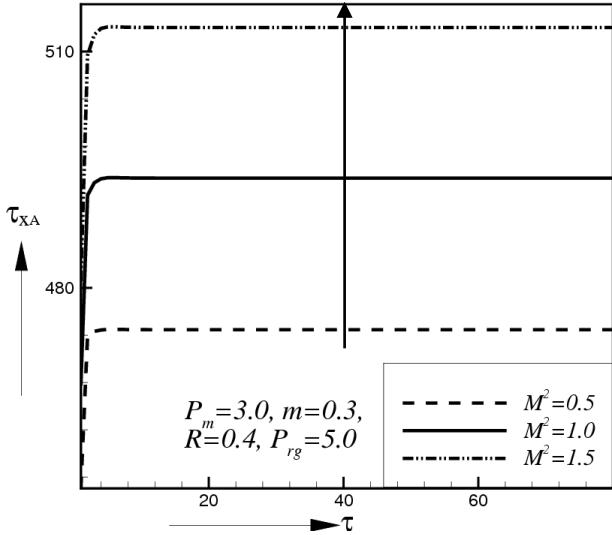


Fig.36. Steady-state average shear stress in  $x$  – direction for different values of  $M^2$  at  $\theta = 45^\circ$  in case of moving plate

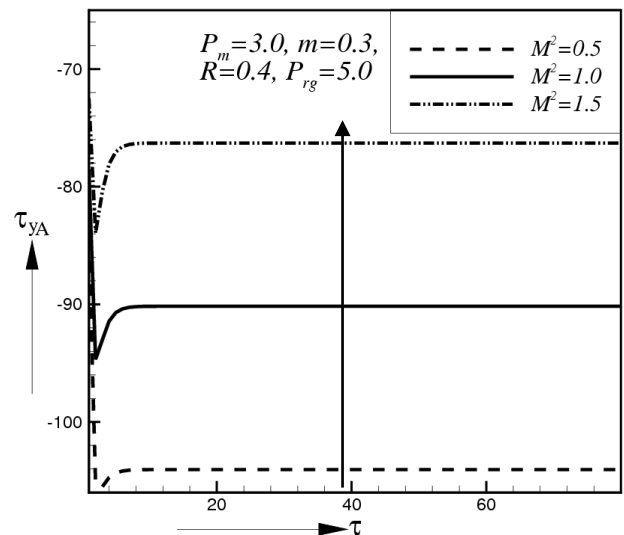


Fig.37. Steady-state average shear stress in  $y$  – direction for different values of  $M^2$  at  $\theta = 45^\circ$  in case of moving plate

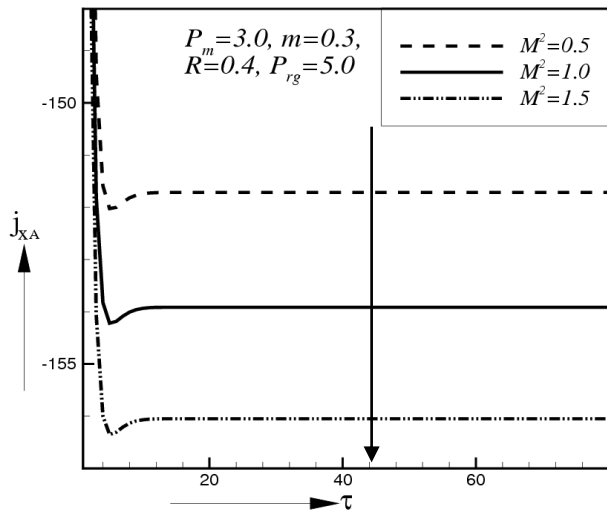


Fig.38. Steady-state average current density in  $x$  – direction for different values of  $M^2$  at  $\theta = 45^\circ$  in case of moving plate

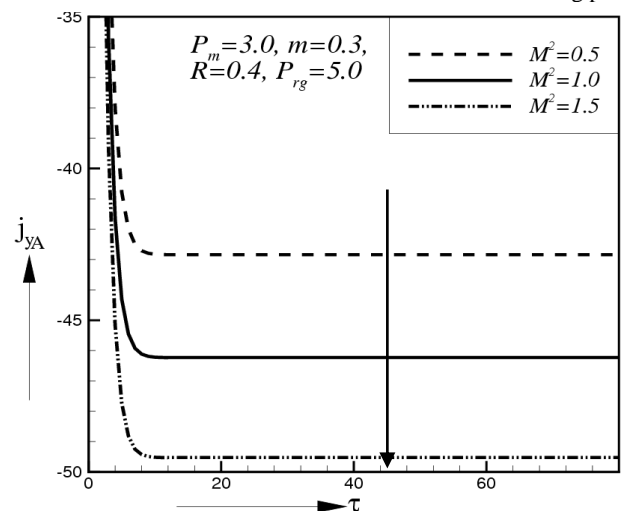


Fig.39. Steady-state average current density in  $y$  – direction for different values of  $M^2$  at  $\theta = 45^\circ$  in case of moving plate

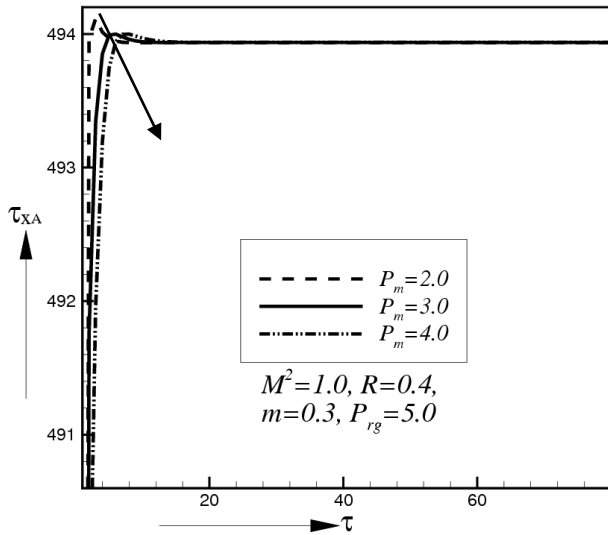


Fig.40. Steady-state average shear stress in  $x$  – direction for different values of  $P_m$  at  $\theta = 45^\circ$  in case of moving plate

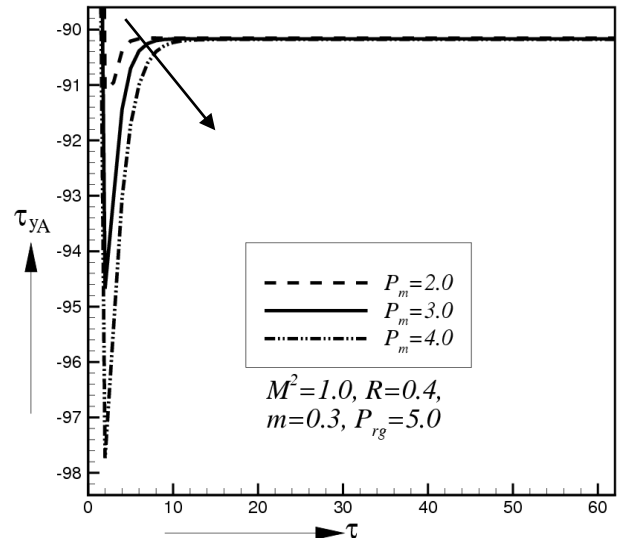


Fig.41. Steady-state average shear stress in  $y$  – direction for different values of  $P_m$  at in case of moving plate  $\theta = 45^\circ$

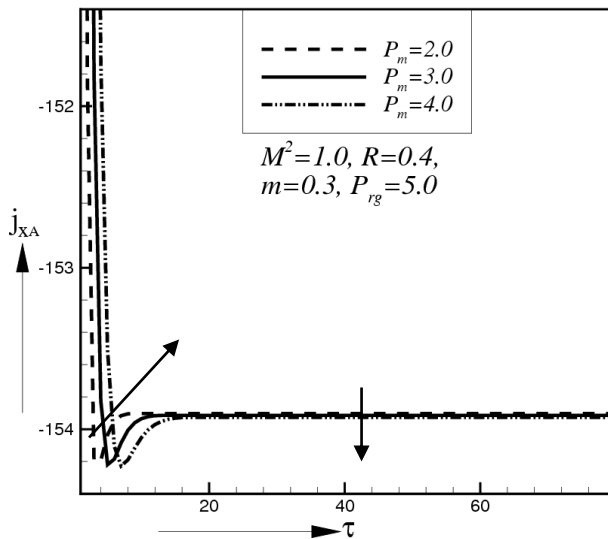


Fig.42. Steady-state average current density in  $x$  – direction for different values of  $P_m$  at  $\theta = 45^\circ$  in case of moving plate

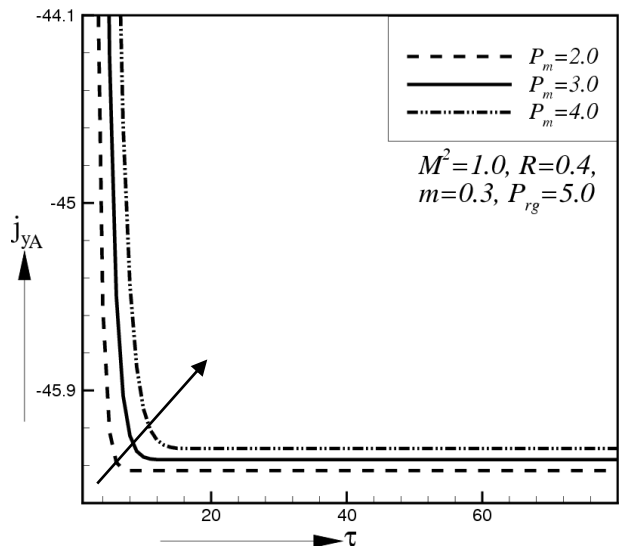


Fig.43. Steady-state average current density in  $y$  – direction for different values of  $P_m$  at  $\theta = 45^\circ$  in case of moving plate

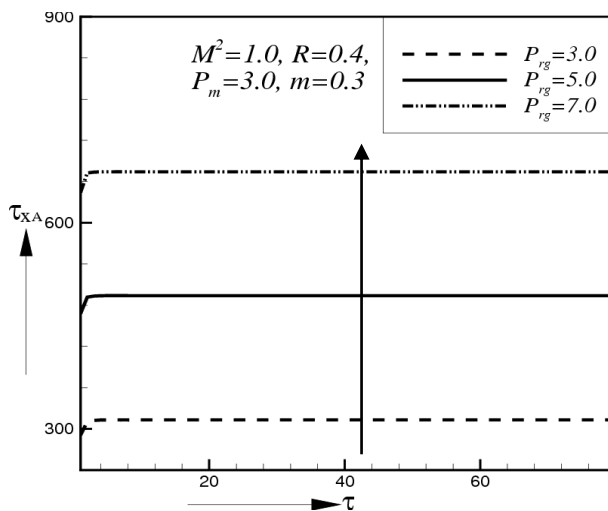


Fig.44. Steady-state average shear stress in  $x$  – direction for different values of  $P_{rg}$  at  $\theta = 45^\circ$  in case of moving plate

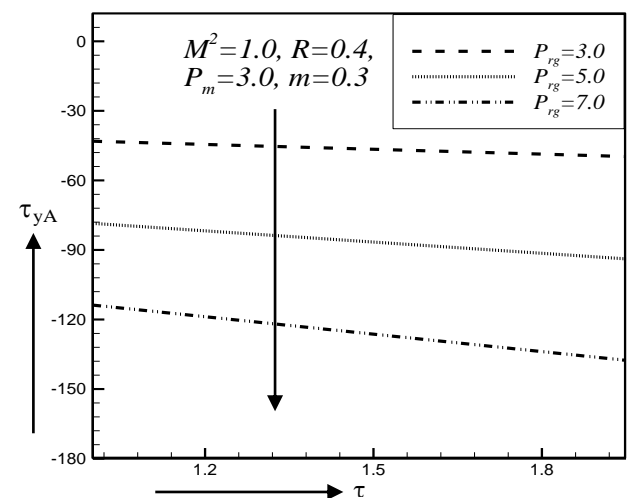


Fig.45. Steady-state average shear stress in  $y$  – direction for different values of  $P_{rg}$  at  $\theta = 45^\circ$  in case of moving plate

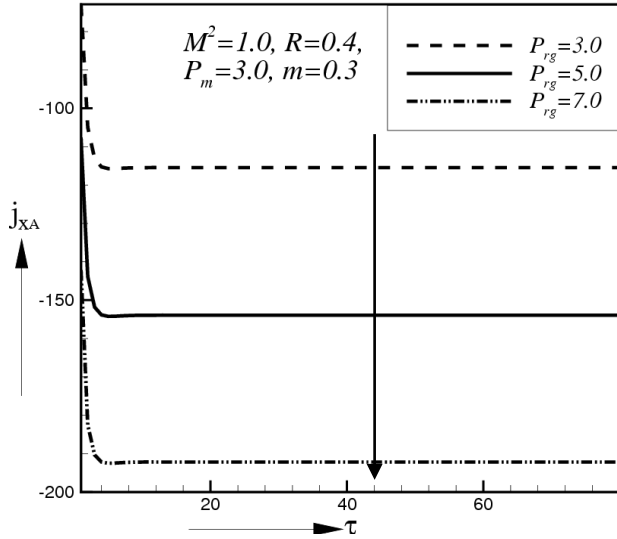


Fig.46. Steady-state average current density in  $x$  – direction for different values of  $P_{rg}$  at  $\theta = 45^\circ$  in case of moving plate

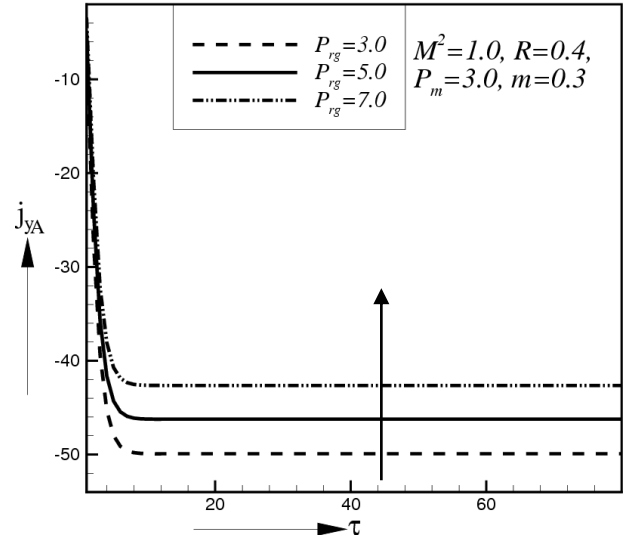


Fig.47. Steady-state average current density in  $y$  – direction for different values of  $P_{rg}$  at  $\theta = 45^\circ$  in case of moving plate

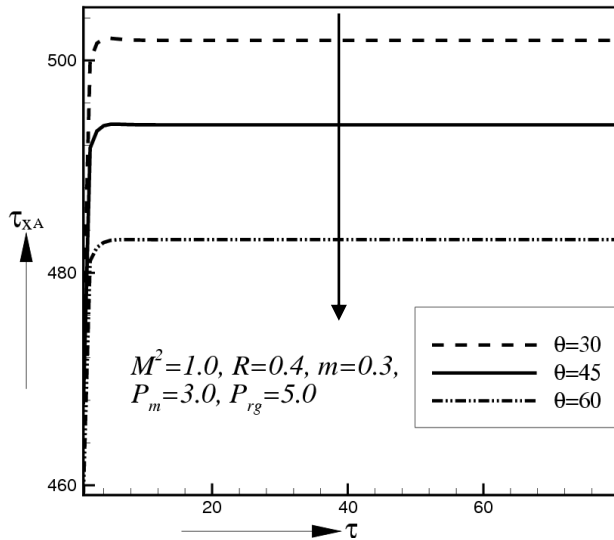


Fig.48. Steady-state average shear stress in  $x$  – direction for different values of  $\theta$  in case of moving plate

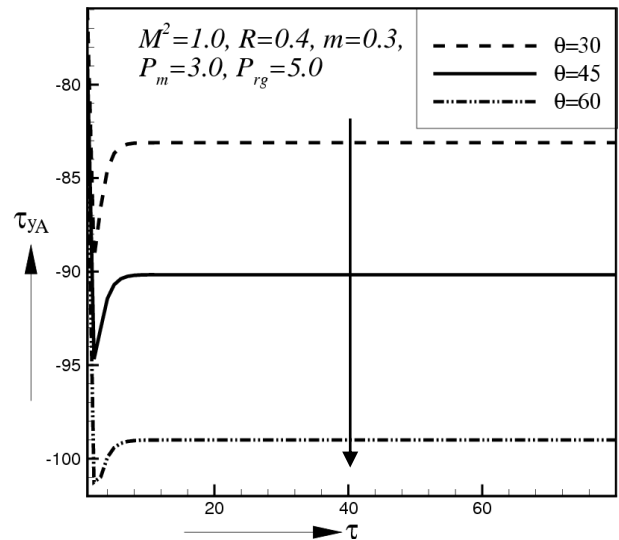


Fig.49. Steady-state average shear stress in  $y$  – direction for different values of  $\theta$  in case of moving plate

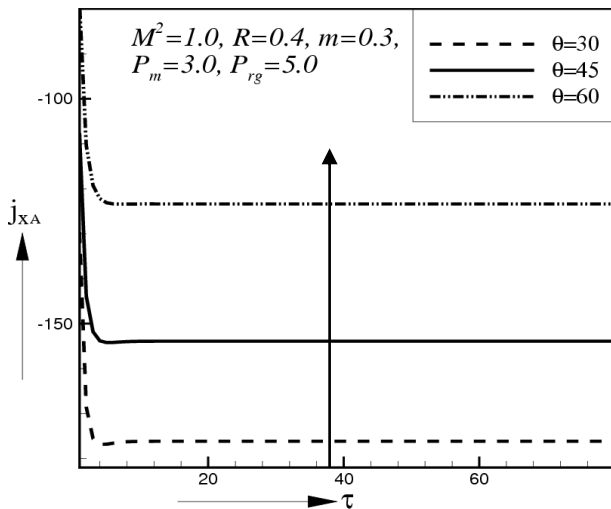


Fig.50. Steady-state average current density in  $x$  – direction for different values of  $\theta$  in case of moving

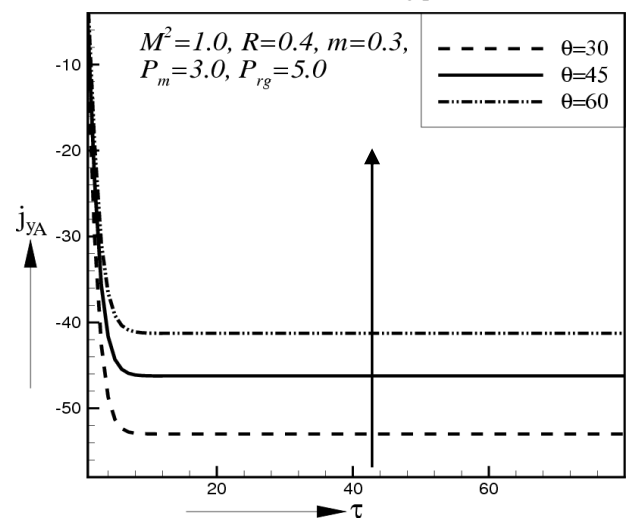


Fig.51. Steady-state average current density in  $y$  – direction for different values of  $\theta$  in case of moving plate

## Conclusions

The explicit finite difference solutions of fluid flow through parallel plates in the presence of hall current with inclined magnetic field in a rotating system for  $\theta = 45^0$  is investigated. Some important findings of this investigation are listed below.

1. The local shear stress profiles in  $x$ –direction in case of moving plate decrease with the increase of  $R, m, P_m$  and  $\theta$  and increase with the increase of  $M^2$  and  $P_{r_g}$ .
2. The local shear stress profiles in  $y$ –direction in case of moving plate decrease with the increase of  $R, m, P_m, P_{r_g}$  and  $\theta$  and increase with the increase of  $M^2$ .
3. The local current density profiles in  $x$ –direction in case of moving plate increase with the increase of  $R, m$  and  $\theta$ , decrease with the increase of  $M^2$  and  $P_{r_g}$  and have minor effect for  $P_m$ .
4. The local current density profiles in  $y$ –direction in case of moving plate increase with the increase of  $R, P_m, P_{r_g}$  and  $\theta$  and decrease with the increase of  $m$  and  $M^2$ .
5. The average shear stress profiles in  $x$ –direction in case of moving plate decrease with the increase of  $R, m, P_m$  and  $\theta$ , increase with the increase of  $M^2$  and  $P_{r_g}$ .
6. The average shear stress profiles in  $y$ –direction in case of moving plate decrease with the increase of  $R, m, P_m, P_{r_g}$  and  $\theta$  and increase with the increase of  $M^2$ .
7. The average current density profiles in  $x$ –direction in case of moving plate increase with the increase of  $R, m$  and  $\theta$ , decrease with the increase of  $M^2$  and  $P_{r_g}$  and have cross flow effect for  $P_m$ .
8. The average current density profiles in  $y$ –direction in case of moving plate increase with the increase of  $R, P_m, P_{r_g}$  and  $\theta$  and decrease with the increase of  $m$  and  $M^2$ .

The findings may be useful for the study of movement of oil or gas, producing electricity; these results are also of great interest in geophysics, astrophysics and fluid engineering. As the basis of many scientific and engineering applications, for studying more complex problems involving the flow of electrically conducting fluids, it is assumed that the present investigation of fluid flow in the presence of inclined magnetic field with hall current in a rotating system can be utilized.

## References

1. Cowling, T. G., (1957), "Magnetohydrodynamics", *Interscience Publications*, New York.
2. Cramer K.R. and Pai S.I.,(1973), "MagnetofluidDynamics for Engineers and Applied Physicists", *McGraw-Hill*, New York.
3. Edmad M. Aboeldahab, Elsayed M.E Elbarbary, "Hall current effect on magneto hydrodynamic free convection flow past a semi-infinite vertical plate with mass transfer", *International Journal of Engineering Science*, **Vol. 39**, pp.1641(2005).
4. Ghosh, S.K. and Bhattacharjee, P.K., "Hall Effects on Steady Hydrodynamic Flow in a Rotating Channel in the Presence of an Inclined Magnetic Field," *Czechoslovak Journal of Physics.*, **Vol. 50**, pp.759(2000).
5. Jha B.K. and Apere C.A., " Combined effect of Hall and Ion-Slip Currents on Unsteady MHD Couette Flows in a Rotating System," *journal of Physical Society of Japan*, **Vol. 79**, No.10,2010,pp104401(2010).
6. Satttar, M. A. and Alam, M. M., "MHD free convective heat and mass transfer flow through a porous medium near an infinite vertical porous plate with Hall current and constant heat flux", *Indian Journal of Pure and Applied Mathematics*, **Vol. 26**, pp. 157(1995).
7. Seth G.S., Raj Nandkeolyar and Md. S. Ansari, "Hartmann Flow in a Rotating System in the Presence of Inclined Magnetic Field with Hall Effects", *Tamkang Journal of Science and Engineering*, **Vol. 13**,No.3, pp.243(2010).
8. Haque, M. M. and Mahmud Alam, MD., "Transient heat and mass transfer by mixed convection flow from a vertical porous plate with induced magnetic field, constant heat and mass fluxes", *AMSE Journals, Modelling B, Measurement and Control, Mechanics and Thermics*, Vol. 78, N° 3/4, (2009).
9. Sutton, G.W. and Sherman, a., "Engineering Magnetohydrodynamics", *New York: McGraw-Hill*(1965).
10. Ziaul Haque, Md. and Mahmud Alam, MD., "Micropolar fluid behaviours on unsteady MHD heat and Mass transfer flow with constant heat and mass fluxes, joule heating and viscous dissipation", *AMSE Journals, Modelling B, Measurement and Control, Mechanics and Thermics*, Vol. 80, N° 1/2, (2011).